Composite Structures 321 (2023) 117303

Contents lists available at ScienceDirect

Composite Structures

journal homepage: www.elsevier.com/locate/compstruct

Material parameter optimization of flax/epoxy composite laminates under low-velocity impact

Valentina Giammaria [a,*], Giulia Del Bianco [a], Elena Raponi [b,c], Dario Fiumarella [d], Raffaele Ciardiello [d], Simonetta Boria [a], Fabian Duddeck [b], Giovanni Belingardi [d]

[a] School of Science and Technology, Mathematics division, University of Camerino, Via Madonna delle Carceri 9, 62032 Camerino, Italy
[b] School of Engineering and Design, Technical University of Munich TUM, Arcisstr. 21, 80333 Munich, Germany
[c] Sorbonne Université, CNRS, LIP6, 4 Place Jussieu, 75005 Paris, France
[d] Department of Mechanical and Aerospace Engineering, Politecnico di Torino, Corso Duca degli Abruzzi 24, 10129 Torino, Italy

ARTICLE INFO

Keywords:
Natural-fiber composites
Impact behavior
Finite element analysis
Efficient global optimization
Surrogate models
LS-OPT

ABSTRACT

Since natural fibers have great potential as an alternative to synthetic fibers when the components are impacted at low energies, their mechanical properties under different types of loads need to be investigated. This can be accomplished by using finite element analysis, which is based on the definition of numerical models that reproduce the objects of the physical phenomenon under study. In defining these models, many parameters of the material cards are determined by experimental tests. However, experiments are time-consuming and costly, and it is not always possible to perform all the necessary tests to determine the values for all unknown parameters. For this purpose, the trial-and-error method is usually used. In this work, we present an optimization procedure for predicting the behavior of flax/epoxy composite laminates under low-velocity impact, using the LS-DYNA solver for numerical simulation. The study aims at identifying the values of relevant parameters that allow for predicting the experimental force–displacement trend as accurately as possible and reproducing the damage mechanisms numerically. Each step of the optimization flow is performed with the external tool LS-OPT, using dynamic time warping as a similarity measure to efficiently handle noise. For this purpose, we use the Efficient Global Optimization algorithm, a strategy based on surrogate modeling techniques. We address a multi-target scenario, i.e., we consider several energy levels simultaneously, aiming to find an optimal parameter configuration that is less sensitive to variations in impact energy. The results obtained not only demonstrate the potential of surrogate-based optimization to identify material parameters, but also provide a characterization of the studied composite configuration in view of future applications.

1. Introduction

Polymer composites are widely used in most industries, such as automotive, construction, marine, wind energy, packaging, and sports, and their demand is increasing over the years thanks to the possibility of combining high mechanical properties with lightness in structural components [1]. This leads to significant use of synthetic materials, i.e., polymeric matrices and synthetic fiber reinforcements, and thus to major problems of disposal at the end of their life cycle, as they are not biodegradable. An alternative is to exploit the biodegradability of natural materials, driving attention to natural fibers of vegetable origin as reinforcing materials for composites. In automotive components, for example, natural-fiber composites can improve fuel efficiency and reduce pollutant emissions during vehicle operation. In addition, the production of natural fibers is more environmentally friendly than that of synthetic fibers, and energy is recovered when natural fibers are burned at the end of their life [2]. In general, fibers such as flax, hemp, and jute can offer high specific mechanical properties combined with low cost, renewability, and biodegradability [3]. In addition, they enable a reduction in energy consumption and CO_2 emissions compared to synthetic fibers, as shown by published results on the life cycle assessment of flax [4], hemp [5] and china reed [2].

Flax is one of the most widely used natural fibers in composite laminates. They offer the best potential combination of low cost, light weight, high strength, and stiffness for structural applications, making them a comparable and potential substitute for glass fibers in many

* Corresponding author.
E-mail addresses: valentina.giammaria@unicam.it (V. Giammaria), giulia.delbianco@unicam.it (G. Del Bianco), elena.raponi@tum.de (E. Raponi), dario.fiumarella@polito.it (D. Fiumarella), raffaele.ciardiello@polito.it (R. Ciardiello), simonetta.boria@unicam.it (S. Boria), duddeck@tum.de (F. Duddeck), giovanni.belingardi@formerfaculty.polito.it (G. Belingardi).

https://doi.org/10.1016/j.compstruct.2023.117303
Received 8 October 2022; Received in revised form 30 April 2023; Accepted 22 June 2023
Available online 26 June 2023

engineering applications [6–8]. Several studies on hybridization of flax fibers with basalt [9,10], carbon fibers [11], and glass fibers [12–15] show promising structural performance of flax fiber-reinforced polymer composites in terms of durability, mechanical properties, and fire behavior. In addition, a characterization of the impact behavior of flax/epoxy composites at different temperatures and an evaluation of the residual flexural properties of these composites are given in [16,17].

Numerical simulations can contribute to a deeper understanding of the mechanical properties of flax fiber composites to further reduce component production costs and better utilize natural fiber-reinforced polymer composites in engineering applications [7]. Several numerical modeling studies for flax fabric-reinforced polymer composites can be found in the literature. A few examples are the following: Liang et al. [18] proposed a model to predict the tensile properties of unidirectional laminates reinforced with flax fabric, Poilâne et al. [19] investigated the viscoelastic behavior of unidirectional flax fabric-polymer composites using numerical models, Assarar et al. [20] focused on the simulation of vibration damping of multilayer flax-carbon composites in the framework of plate theory, Sliseris et al. [7] developed a micromechanical numerical model for both flax short fiber and flax fiber fabric reinforced polymer composites. A subcategory of numerical studies deals with low-velocity impact (LVI) tests [7,21,22], which are of particular interest because they are especially damaging to composite components as they can cause degradation of mechanical properties while remaining undetected at visual inspection [23]. In this type of test, specimens are subjected to various impact energies to progress from barely visible impact damage to perforation, with the ultimate goal of evaluating damage mechanisms and residual properties.

To the authors' knowledge, there are still no optimization studies in the literature for fine-tuning the material card parameters of flax-fiber/epoxy-resin composite laminates subjected to low-velocity impact. This is a first but essential step for any optimization study aimed at improving the performance of complete mechanical components, especially when modeling the mechanical properties of reinforced natural fiber composites. As suggested by Mulenga et al. [24], this is a complex process due to various parameters such as the type of matrix/fiber used, the overall composition, the manufacturing process, etc. Efficient Global Optimization (EGO) [25] is one of the most powerful existing approaches for global optimization using response surfaces. It is particularly suitable for the optimization of black-box problems – i.e., problems with no explicit formulation of the objective function to be optimized – where only a limited budget of function evaluations is available. This is the case for the optimization of parameters in a numerical model, where each objective function evaluation is computationally expensive since it is read from the output of a finite element numerical simulation.

This paper focuses on an optimization study performed on flax/epoxy composite laminates impacted at three energies – 5 J, 10 J, and 15 J – using the commercial software LS-OPT [26]. In particular, the main objective of the optimization strategy is the numerical characterization of the material in order to achieve a uniform parameter configuration, regardless of the energy level tested. To characterize the material, we first perform a series of experimental tests, including tensile tests, four-point bending tests, and LVI tests. Second, we design a finite element impact model and simulate it using explicit software LS-DYNA [27], which provides different damage mechanic material models for composites. In this study, we use a MAT54/55 card [28], described in Section 4. Then, we perform a sensitivity analysis to select the parameters with the greatest influence on the output response. Finally, we use EGO to find the parameter configuration that best reproduces the experimental load–displacement curves for the different impact energies. Here we consider a multi-target approach aimed at obtaining satisfactory results for multiple energy levels, which we believe is a good practice to achieve a good level of generalization in material characterization. As we will show in Section 7.2, optimization based on a single test case is indeed not a reliable technique, since the parameters obtained do not give accurate results for impacts at other energy levels.

The comparison between the numerical and experimental results shows a good agreement and a significant improvement over the curves obtained by simulating the models tuned by trial and error. Therefore, our multi-target, surrogate-based optimization strategy not only proves to be effective in identifying the material parameters of the specific numerical model, but also generalizes well over different boundary conditions. With this work, we provide a material characterization for flax/epoxy composites modeled through a MAT54/55 material card. We show that, although this card was introduced specifically for unidirectional laminates, it can satisfactorily reproduce the impact behavior with much fewer parameters than, for example, a MAT058 for woven composites.

2. Materials

Composite laminates were produced by HP Composites SpA using a PrePreg composed of a flax woven fabric and epoxy resin. The flax reinforcement was balanced (weight distribution: 50% warp and 50% weft), with 5 threads/cm for the weft and 6 threads/cm for the warp, a fiber architecture of twill 2 × 2, and a weight of 350 g/m^2. The curing cycle was performed in autoclave at 135 °C for 90 min under 6 bar, with a vacuum bag on the components. An initial heating ramp and a final cooling ramp provided a gradual thermal process with low heating (3 °C/min) and cooling (4 °C/min) rates to achieve a uniform temperature distribution and avoid deformation of the specimens. In this work, we analyze the following two configurations:

- single lamina, for mechanical tensile characterization only: 1 layer with orientations of 0°, 45°, and 90°. The average measured thickness is 0.6 mm;
- laminates: 8 layers with the same stacking sequence and a total average thickness of 3.68 mm, for which three different orientations are considered: 0°, 45°, and 90°.

If we look at the two types of specimens and compare their thicknesses, we notice that during the manufacturing process the layers in the laminates became more compact compared to the single laminae. In this case, the resin flow out is favored, resulting in a total thickness that is less than eight times the thickness of the single lamina. The lower resin content in the laminates also affects the mechanical properties, showing better behavior in tensile tests, as reported in Section 3.

3. Experimental tests

3.1. Tensile and four-point bending tests

We used tensile and four-point bending tests to mechanically characterize the specimens. Both tests were performed at Politecnico di Torino on a servo-hydraulic machine (Instron 8801) equipped with a 100 kN load cell. The tensile tests (specimen dimensions of 250 mm × 25 mm) were performed for both laminae and laminates according to ASTM D3039. A test speed of 2 mm/min and a grip pressure of 100 bar were used at a room temperature of approximately 29 °C. For each orientation and type, three specimens were tested, equipped with two grid gauges (type 1-XY38-6/350, from HBM). Four-point bending tests (specimen dimensions of 150 mm × 25 mm) were performed only on laminates conforming to ASTM D6272 with the following setup: a test speed of 2 mm/min, a load span of 30 mm, a support span of 60 mm, so that the ratio of load-to-support span is 1:2. Four specimens were tested for 0° and 90° orientations, while two specimens were tested for 45°.

Tables 1 and 2 summarize the material properties (i.e., maximum stress before failure, and elastic and shear modulus) obtained from the tensile and bending tests, respectively. Figs. 1 and 2 show the

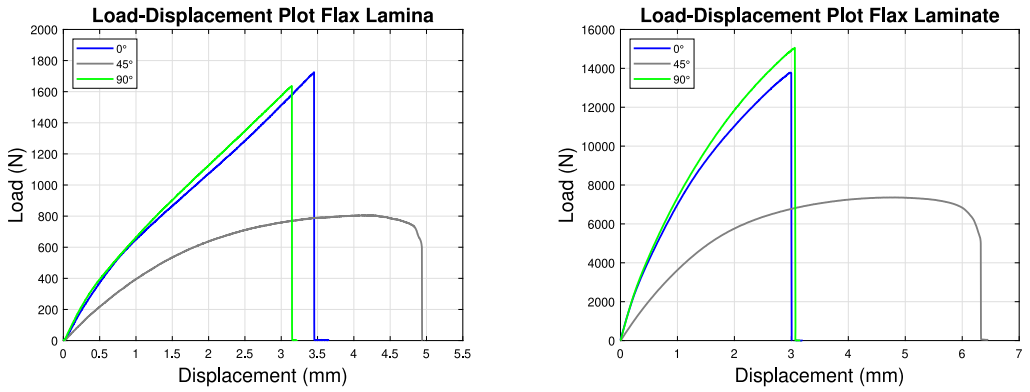

(a) (b)

Fig. 1. Load-Displacement plots of tensile tests. (a) Laminae. (b) Laminates.

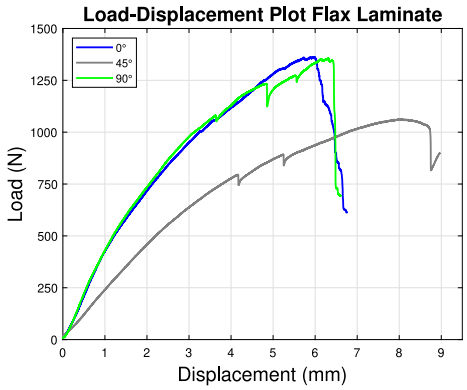

Fig. 2. Load-Displacement plots of bending tests.

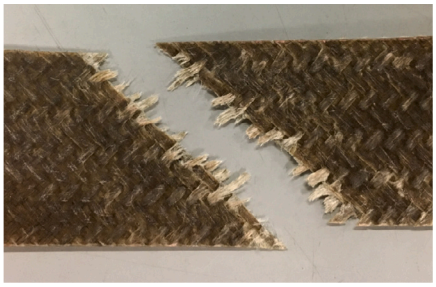

Fig. 3. Flax fiber pullout of a single lamina specimen oriented at 45°.

respective load–displacement plots, with only one curve shown for each orientation and configuration due to the consistency of the different test replicas. All the curves in the 0° and 90° orientations are aligned, confirming the balanced nature of the flax fabric. Moreover, the curves exhibit an initial nonlinear behavior typical of the failure mechanism of natural fibers and related to their viscoelastic nature and the rearrangement of fibrils [29]. Failure occurs after a short yielding phase that ends with fiber pullout. Compared to specimens oriented at 0° and 90°, those oriented at 45° exhibit half the mechanical properties and achieve greater displacement before failure. Fig. 3 shows the tensile failure and the fiber pullout of a single lamina specimen oriented at 45°.

Table 1
Experimental tensile properties of flax specimens. E: Young modulus; σ_u: ultimate strength; G: shear modulus.

	Orientation	E [MPa]	σ_u [MPa]	G [MPa]
Laminae	0°	9592	110.2	
	45°	5609	60.9	1797
	90°	10992	118.1	
Laminates	0°	16079	152.4	
	45°	7330	84.5	2227
	90°	19518	169.9	

Table 2
Experimental bending properties of flax laminates specimens. E_B: Flexural modulus; σ_u: ultimate strength.

Orientation	E_B [MPa]	σ_u [MPa]
0°	12446	163.2
45°	6905	144.5
90°	13251	168.2

3.2. Low-velocity impact (LVI) tests

Impact tests were performed at Politecnico di Torino on laminate specimens oriented at 0°, with dimensions of 100 mm × 100 mm, using a drop tower machine (Instron/CEAST Fractovis Plus) equipped with a hemispherical impactor instrumented with a piezoelectric load cell of 12.7 mm diameter and a total mass of 15.94 kg at room temperature. The samples were clamped between two steel plates with a circular opening of 40 mm diameter. Three different energy levels were tested: 5 J, 10 J, and 15 J, corresponding to initial impactor velocities of 0.8 m/s, 1.13 m/s, and 1.38 m/s, respectively. Five specimens were tested at 10 J, while only two specimens were impacted at the remaining two energy levels, as the observed results were reproducible.

The experimental load–displacement curves at the three impact energy levels are shown in Fig. 4, coupled with the reported crack propagation on the back and the front surfaces, shown in Figs. 5 and 6, respectively. When a sample is subjected to out-of-plane impact, the failure modes are, in order: indentation, delamination, matrix cracking, and fibers breakage. Indentation is more characteristic of ductile and nonbrittle materials, and also depends strongly on the thickness of the specimen. Crack initiation and springback occur at 5 J (Figs. 4(a), 5(a), 6(a)), partial penetration is visible at 10 J (Figs. 4(b), 5(b), 6(b)), and complete perforation is reached at 15 J (Figs. 4(c), 5(c), 6(c)). From Figs. 5(a) and 6(a), we can notice that the slight indentation on the front surface for the 5 J impact is accompanied by delamination on the back surface. The same is true for the impacts at 10 J. It can be seen, however, that the rear surfaces are increasingly

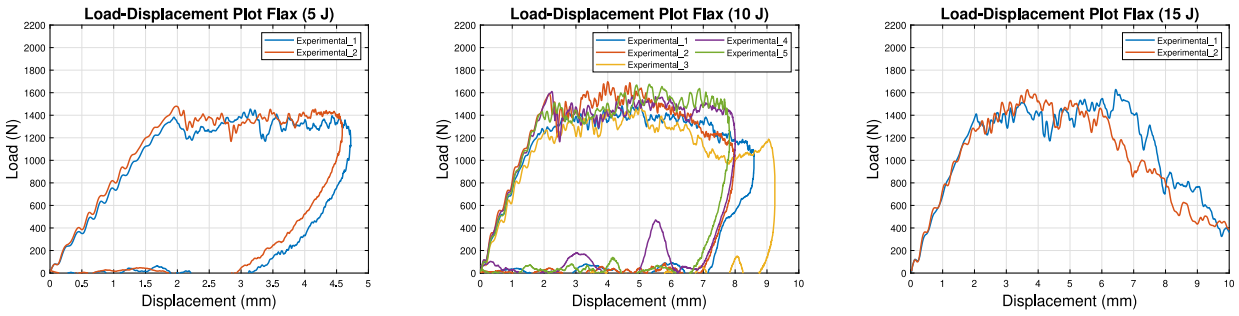

(a) (b) (c)

Fig. 4. Load-Displacement plots for flax samples impacted at (a) 5 J, (b) 10 J, and (c) 15 J.

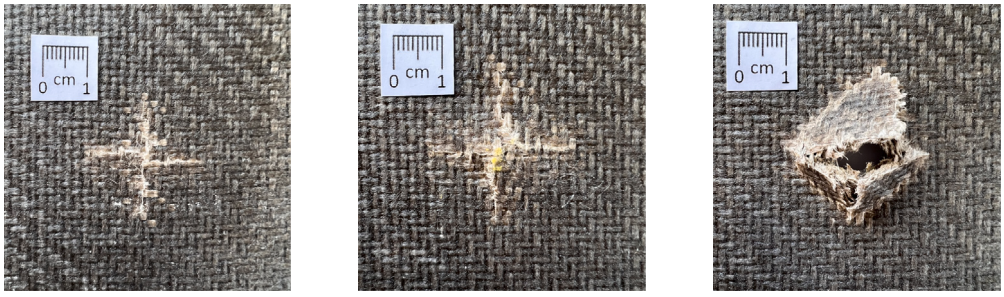

(a) 5 J **(b)** 10 J **(c)** 15 J

Fig. 5. Damage evolution on the back surfaces for flax samples impacted at (a) 5 J, (b) 10 J, and (c) 15 J.

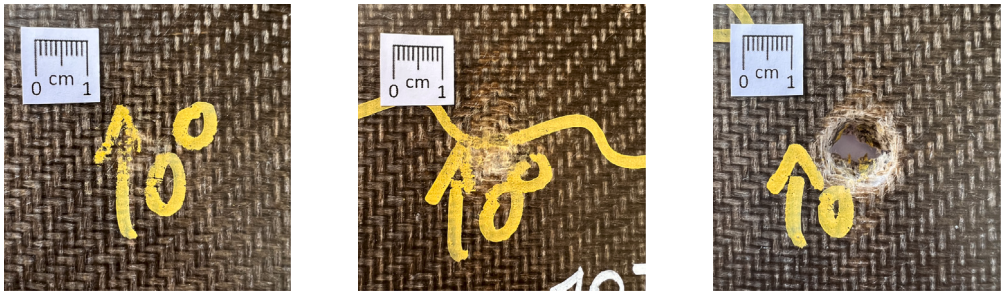

(a) 5 J **(b)** 10 J **(c)** 15 J

Fig. 6. Damage evolution on the front surfaces for flax samples impacted at (a) 5 J, (b) 10 J, and (c) 15 J.

more damaged than the upper ones for all three energies. In particular, in the case of 10 J, delamination is widespread in the back area (Fig. 5(b)), while the front region damaged by indentation is almost limited to the diameter of the impactor (Fig. 6(b)). As the impact energy increases, the effect of damage due to delamination visible on both the sample surfaces becomes larger. In particular, the cross-shaped crack along the warp and weft direction of the fabric is clearly visible on the back surfaces in Figs. 5. This phenomenon is attributed to the high densification of the laminates, which allows for perfect right-angled failure modes.

4. Numerical modeling

The finite element model for the LVI on the flax/epoxy laminates was created using Altair HyperMesh and simulated using the explicit finite element analysis solver LS-DYNA [27].

The numerical model we propose consists of 4 composite shell layers (PART_COMPOSITE), each of which with 2 integration points through the thickness in order to reproduce the 8 layers of the specimen. The model is shown in Fig. 7 and has a total thickness for the 8 plies of 3.68 mm so that each modeled ply is 0.46 mm thick. A fine mesh with an element size of 0.9 mm was used to discretize the square central impact zone, while a mesh with a gradually larger element size characterize the remaining area, in order to reduce the simulation times. The MAT54/55 material model (MAT_ENHANCED_COMPOSITE_DAMAGE) was used for the flax/epoxy composite. This material card is properly formulated to reproduce the brittle behavior of unidirectional fibers, with Chang-Chang failure criterion. Element deletion is strain-based: once all integration points exceed one of the strain parameters, failure occurs in the composite layers and the element is deleted. Hence, the elements adjacent to the deleted one become crash-front elements. Among the damage-based constitutive models provided by LS-DYNA to describe composites [28,30], MAT54/55 is the most common one used in crash simulations. In addition, compared to MAT058 and MAT262, it requires a smaller number of input parameters and is therefore much easier to set. For this reason, although our reinforcement is a fabric, MAT54/55 is a good compromise between accuracy and computational cost, especially when an optimization strategy must be performed. The impactor is spherical, has a mass of 15.94 kg, and is modeled as a rigid body with solid elements using a MAT20 material card (MAT_RIGID). To analyze the contact

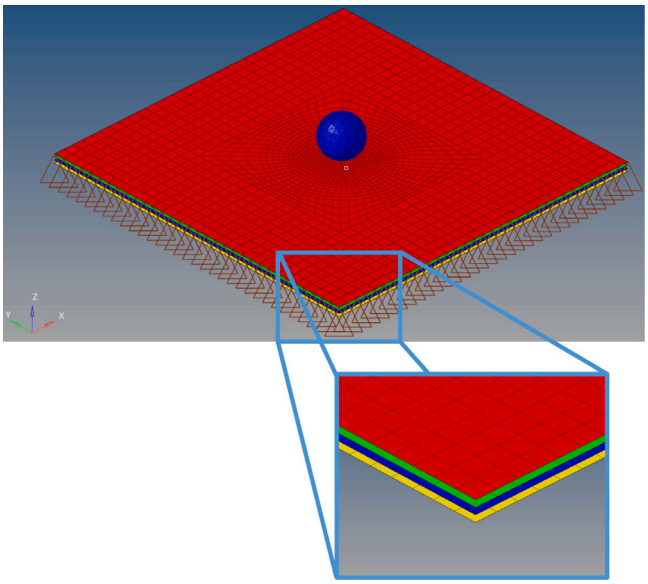

Fig. 7. Numerical impact model, with a close-up of the layers.

between the master and slave surfaces during the crash, a contact (CONTACT_SURFACE_TO_SURFACE) was imposed between the impactor and the laminates. In addition, three tie-break contacts (CONTACT_AUTOMATIC_ONE_WAY_SURFACE_TO_SURFACE_TIEBREAK) connect the 4 modeled plies and describe their interlaminar interactions. The three initial impactor velocities, corresponding to the three tested energy levels, are set as boundary conditions, while all nodes outside the unconstrained impact zone are constrained with an interlocking. The same model is used for all impact energy cases, changing the initial velocity of the sphere. For a more detailed discussion of the required parameters in the material card, the numerical results, and their comparison with experimental results, see Section 7.

5. Sensitivity analysis

Since the MAT54/55 material card in LS-DYNA requires the definition of several parameters, we perform an initial screening to reduce the number of design variables and thus the computational time for the optimization run. We investigate the influence of five variables (DFAILM, DFAILT, DFAILC, DFAILS, and XC) to identify which of them heavily influences the low-velocity impact response. They correspond to the maximum matrix strain in tension or compression (DFAILM), the maximum strain for fiber tension (DFAILT) and compression (DFAILC), the maximum shear strain (DFAILS) and the longitudinal compressive strength (XC). We select these factors because DFAILM, DFAILC, and XC are not available from our experimental campaign, while DFAILT and DFAILS need to be further investigated because (i) their variation in trial-and-error tuning attempts lead to large variations in the results and (ii) the use of their experimental values is not reasonable in this particular case because the architecture of our samples is a woven fabric (twill 2 × 2), whereas the MAT54/55 material card is defined only for unidirectional fibers. For this reason, it is important to highlight the real meaning of the MAT54/55 parameters in the case of woven fabric: While DFAILT refers to the longitudinal direction, DFAILM assumes the same role as DFAILT, i.e., the maximum tensile strain for the fiber, but in the transverse direction. This choice is closely related to the need to use a simpler material card that does not require a large number of parameters to determine, thus reducing the computational time for optimization. We begin with a Design of Experiments (DoE) [31], where a full-factorial sampling technique is chosen, considering two levels for each variable, hence leading to a total number of $2^5 = 32$ DoE points. We perform a sensitivity study for all available energy configurations.

The results obtained are discussed in Section 7.1, where we present main effect and interaction plots for all factors. The main effect plot is used to compare the relative strength of the effects of the different factors, while the interaction plots show the relationship between each pair of factors.

6. Optimization

6.1. Efficient global optimization

EGO [25] is an iterative and adaptive algorithm for black-box problems, i.e., problems for which we do not have an explicit formulation of the objective or its derivatives, that aims to achieve a near-optimal solution with a small budget of evaluations. It starts by fitting a surrogate model to a set of initial points sampled according to a DoE scheme. In this work, the DoE sampling scheme is a space-filling design and the response surface is constructed using a Kriging surrogate model [31]. After fitting the initial response surface to the training set – DoE points and associated objective function values – a new point, referred to as *infill point*, is selected at each iteration by maximizing an Expected Improvement (EI) function defined as follows:

$$EI(\boldsymbol{x}) = \begin{cases} (y_{min} - \hat{y}(\boldsymbol{x}))\ \boldsymbol{\Phi}\left(\frac{y_{min}-\hat{y}(\boldsymbol{x})}{\hat{s}(\boldsymbol{x})}\right) + \hat{s}(\boldsymbol{x})\ \phi\left(\frac{y_{min}-\hat{y}(\boldsymbol{x})}{\hat{s}(\boldsymbol{x})}\right) & \text{if } \hat{s}(\boldsymbol{x}) > 0, \\ 0 & \text{if } \hat{s}(\boldsymbol{x}) = 0. \end{cases} \tag{1}$$

In Eq. (1), $\hat{y}$ is the function that approximates the real and expensive objective function, y_{min} is the best objective function value observed in all previous iterations, $\hat{s}$ is the standard deviation of the model, representing the uncertainty of the interpolated function value, while $\boldsymbol{\Phi}$ and ϕ are the cumulative Gaussian distribution function and the probability density function, respectively. The error in the approximation $\hat{s}$ is used to balance local and global search. According to Eq. (1), the EI can be large due to one of the two additive terms—the first is determined by the prediction mean and the other by the prediction variance. Hence, EI allows locating new points in promising areas, near locations where the best value of the fitness function was computed, and in sparsely populated areas characterized by low sample density and consequently high uncertainties.

The point with the maximum EI is evaluated to update the Kriging model, i.e., a FEM simulation is performed and the objective function value associated with the output is compared to one of the best samples up to the current iteration and used to expand the training set to which the response surface is fitted. The infill procedure is repeated until a termination criterion is met, e.g., a predetermined number of evaluations is reached.

6.2. Dynamic time warping

Dynamic Time Warping (DTW) is one of the methods available in LS-OPT to calculate the distance between two curves. Only recently (from LS_OPT version 6), DTW has been introduced in parameter identification problems as a powerful method for matching simulated and experimental plots. It considers both the shape and the discrepancy between two curves in the abscissa direction, unlike the mean squared error (MSE) which only considers the pointwise difference in the ordinates. The distance between two datasets is computed through a warping path, which represents the minimum cumulative distance required to traverse all points in the curves. If the curves have not the same length, as in this case, the option `Truncate computed using target` must be selected [26], leading to the Partial Dynamic Time Warping (DTW-p) method. As the name

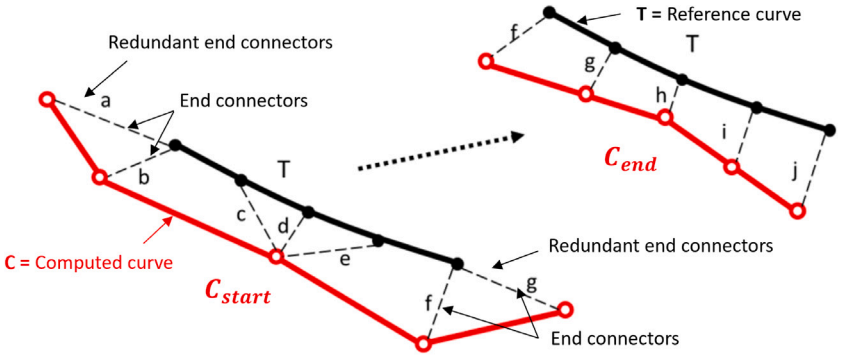

Fig. 8. Scheme of the evolution of DTW-p method. C_{start} refers to the initial computed curve, whereas C_{end} corresponds to the modified computed curve at the end of the procedure [32].

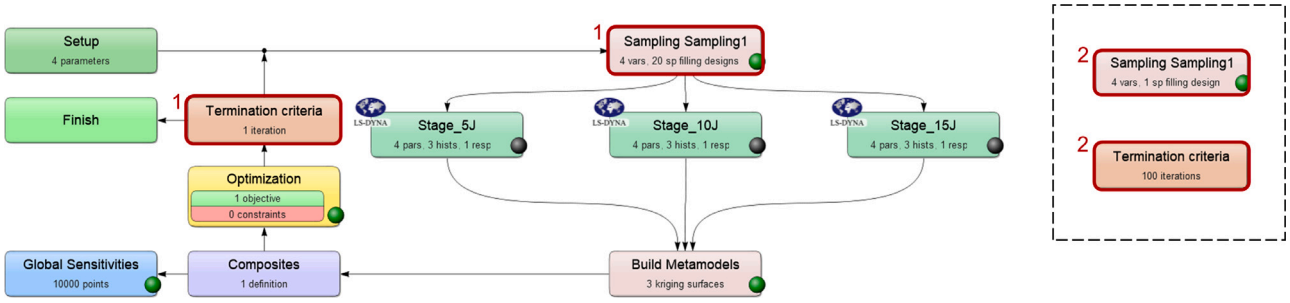

Fig. 9. Optimization flowchart in LS-OPT for the EGO strategy. Red frames highlight the blocks that differ for the two steps of the optimization strategy.

suggests, DTW works in a loop that iterates until both curves have the same number of vertices.

As suggested by Witowski in [32], the method assumes a reference curve (T) and a computed curve (C) (see Fig. 8) and is based on the fact that if one curve is much longer than the other, this means that there are redundant end connectors, i.e., there are multiple end connectors associated with the same endpoint of the reference curve. In these cases, the algorithm trims the curve until there is no redundant end connector left. Once the curves become comparable, the distance is calculated using the standard DTW measure, i.e. by adding the connector lengths and dividing by the number of links. Therefore, with reference to Fig. 8, the distance between the two curves is expressed by the following relation: $(f + g + h + i + j)/5$. For the algorithm to work smoothly, the computed curve is remeshed at each cycle in order to have the same number of nodes as the reference curve. Bisectional interpolation can be used for the remeshing so that the original properties of the curve are preserved. The algorithm ends when there are no more superfluous end connectors.

6.3. Setup in LS-OPT

The focus of this section is on a general description of the EGO strategy from a software perspective, without going into too technical detail. LS-OPT is used to perform (i) the sensitivity analysis on the material card parameters DFAILM, DFAILT, DFAILC, DFAILS, XC, and (ii) the optimization of the most influential parameters DFAILM, DFAILC, DFAILS and XC that resulted from the previous sensitivity analysis.

The optimization procedure is performed in two steps, as shown in Fig. 9. The first step consists of a single iteration for the DoE; this involves sampling the design space to have a set of training points on which to evaluate the objective function. In this study, based on our experience, we choose a space-filling design to locate 20 sample points in a four-dimensional search space, within the following variable bounds:

$$\begin{array}{rcccl} 0.01 & \leq & \text{DFAILM} & \leq & 0.15 \\ -0.1 & \leq & \text{DFAILC} & \leq & 0 \\ 0.01 & \leq & \text{DFAILS} & \leq & 0.2 \\ 0.01 & \leq & \text{XC} & \leq & 0.2 \end{array} \tag{2}$$

The training data with the observed responses are then used by a Kriging model to predict the value of the objective function at each point of the search domain. Hence, the EI function is built over the same domain and its optimization provides the infill point to be evaluated through FEM simulation.

Step 2 consists of 100 iterations, with one function evaluation per iteration. An infill point is added at each iteration and the best design is updated only if the simulated infill point has a better objective function value than the previous best design. In either case, the new data is used to update the Kriging approximation model. The infill procedure is repeated until a predetermined number of evaluations is reached [33], which we consider as termination criterion. These two steps also require specifying the histories and responses to be extracted from the simulation. In this case, we are interested in the force–displacement curves, for which a cross-plot between force and displacement as functions of time is needed. Next, we set up a curve-matching between the simulation curve and the experimental curve. To do this, we add a response and select the desired measure to calculate the mismatch between the curves. Here, the Partial Dynamic Time Warping (DTW-p) method, described in Section 6.2, is used. To have a material characterization that does not depend on the boundary conditions, we consider a multi-target approach, inserting three parallel stages in the optimization procedure, one for each energy level (see Fig. 9). The objective is defined as a composite function (available from the Composites dialog option in LS-OPT) corresponding to the sum of the curvematching functions defined for each energy level.

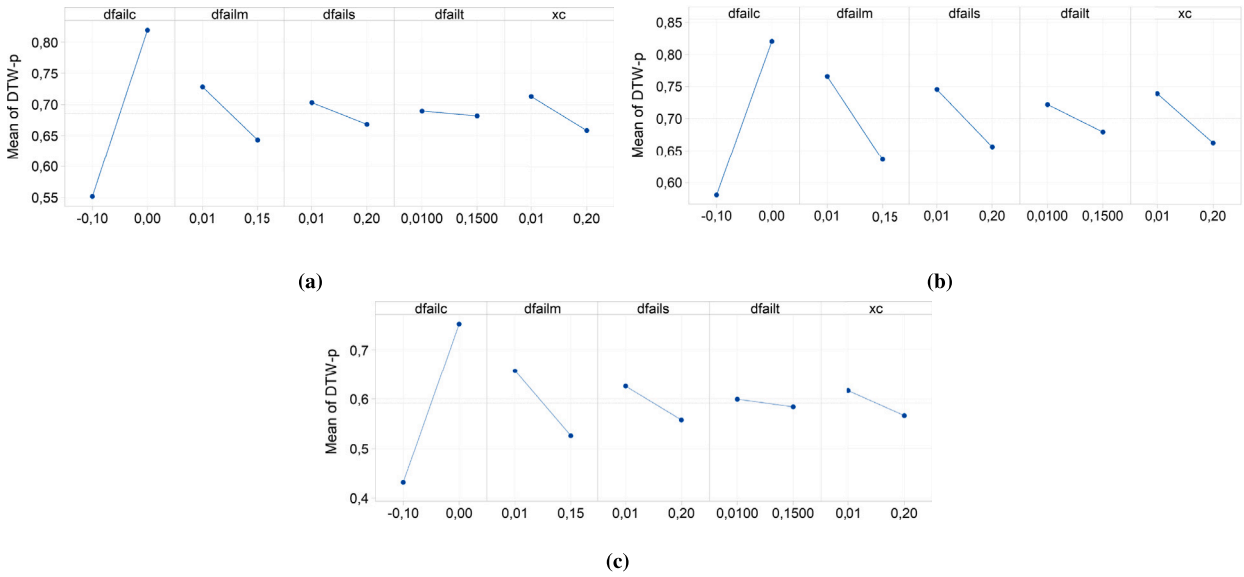

Fig. 10. Main effect plots evaluated on the DTW-p response for Flax cases at (a) 5 J, (b) 10 J, and (c) 15 J.

7. Results and discussion

7.1. Sensitivity analysis

The influence of the five variables (DFAILM, DFAILT, DFAILC, DFAILS, and XC) on the LVI response of flax samples impacted at 5 J, 10 J, and 15 J is here analyzed. The performed full-factorial sensitivity analyses present a high accuracy in terms of R^2: 0.945 for 5 J, 0.955 for 10 J, and 0.905 for 15 J. Figs. 10(a), 10(b), and 10(c) show the relative impact of each input on the DTW-p between the numerical and experimental curves, respectively for each energy level. From these plots, we can see that DFAILC and DFAILM have the greatest influence on the impact response, followed by DFAILS and XC, while the contribution of DFAILT seems to be negligible. The interaction plots in Figs. 11(a), 11(b), and 11(c) show the relationship between each pair of factors and its influence on the response needs. The DFAILT vs DFAILC, DFAILM, and DFAILS plots show straight nearly horizontal lines, confirming that changing DFAILT has little effect on the response. In fact, when the lines are parallel, no interaction between the factors is observed, while non-parallel lines indicate the presence of an interaction: the more non-parallel lines, the stronger the interaction. DFAILC shows a strong interaction with DFAILM, which is also confirmed by the low P-values of the term DFAILC*DFAILM in Table 3. From the table, the second most influential interaction is between DFAILC and DFAILS. For this reason, in this study, we first consider DFAILC, DFAILM, and DFAILS as variables in different optimization runs for different energy levels. Then, we include the factor XC in a multi-target analysis, as it is the third relevant term in the main effects plot and in terms of *P*-value for the 5 J impact energy case. DFAILT is instead set to 0.0885, which is the value found by trial and error.

Table 3
P-values of the full-factorial sensitivity analyses.

		5 J	10 J	15 J
1-Way Interactions	dfailc	0.000	0.000	0.000
	dfailm	0.154	0.022	0.010
	dfails	0.551	0.103	0.153
	dfailt	0.891	0.422	0.737
	xc	0.346	0.151	0.276
2-Way Interactions	dfailc*dfailm	0.180	0.052	0.045
	dfailc*dfails	0.356	0.086	0.376
	dfailc*dfailt	0.940	0.458	0.419
	dfailt*xc	0.543	0.478	0.163
	dfailm*dfails	0.451	0.169	0.181
	dfailm*dfailt	0.790	0.831	0.836
	dfailm*xc	0.837	0.701	0.976
	dfails*dfailt	0.808	0.800	0.912
	dfails*xc	0.800	0.494	0.923
	dfailt*xc	0.844	0.794	0.603

7.2. Material card optimization

We begin our discussion by showing that optimizing the material card independently for each energy level does not give well-generalizable results. Therefore, a multi-target optimization strategy is required.

7.2.1. Single-target optimization

Figs. 10 and 11 show that the objective function is clearly affected by DFAILC, DFAILM, and DFAILS. To account for the influence of all three parameters and their interaction effects, we apply EGO on a three-dimensional domain with the aim of minimizing the discrepancy between the loading phases of the experimental and numerical curves. For each energy level, starting from a space-filling DoE scheme of 15 points, including the parameter configuration (DFAILC, DFAILM, DFAILS) = (−0.06, 0.1, 0.1) determined by trial and error, we run EGO for 80 iterations. We then validate the optimal parameter configuration found by the EGO algorithm for each energy level by running FEM simulations on the other load cases.

Fig. 12 shows the simulation results in the form of load–displacement curves: the green solid curves are from experimental measurements and therefore serve as a reference for the optimization procedure, the red dashed curves refer to the simulations performed with the numerical models tuned by trial and error, and the blue solid curves are from the simulations performed with the models tuned with the optimal parameter configurations found by EGO for the different energy levels. The plots clearly show that the set of optimal parameters found in the optimization for 5 J (Fig. 12(a)) does not give a good prediction for the 10 J (Fig. 12(b)) and 15 J (Fig. 12(c)) cases, where a premature perforation of the sample is observed. Similarly, Figs. 12(d), 12(e), and 12(f), show that the optimal set of parameters found for the 10 J case is not suitable for the 5 J case, where a high peak force and a premature elastic rebound are evident. In addition, according to the plots in Figs. 12(g), 12(h), and 12(i), the optimal parameter set for the 15 J case is not suitable for the 10 J case, where perforation occurs.

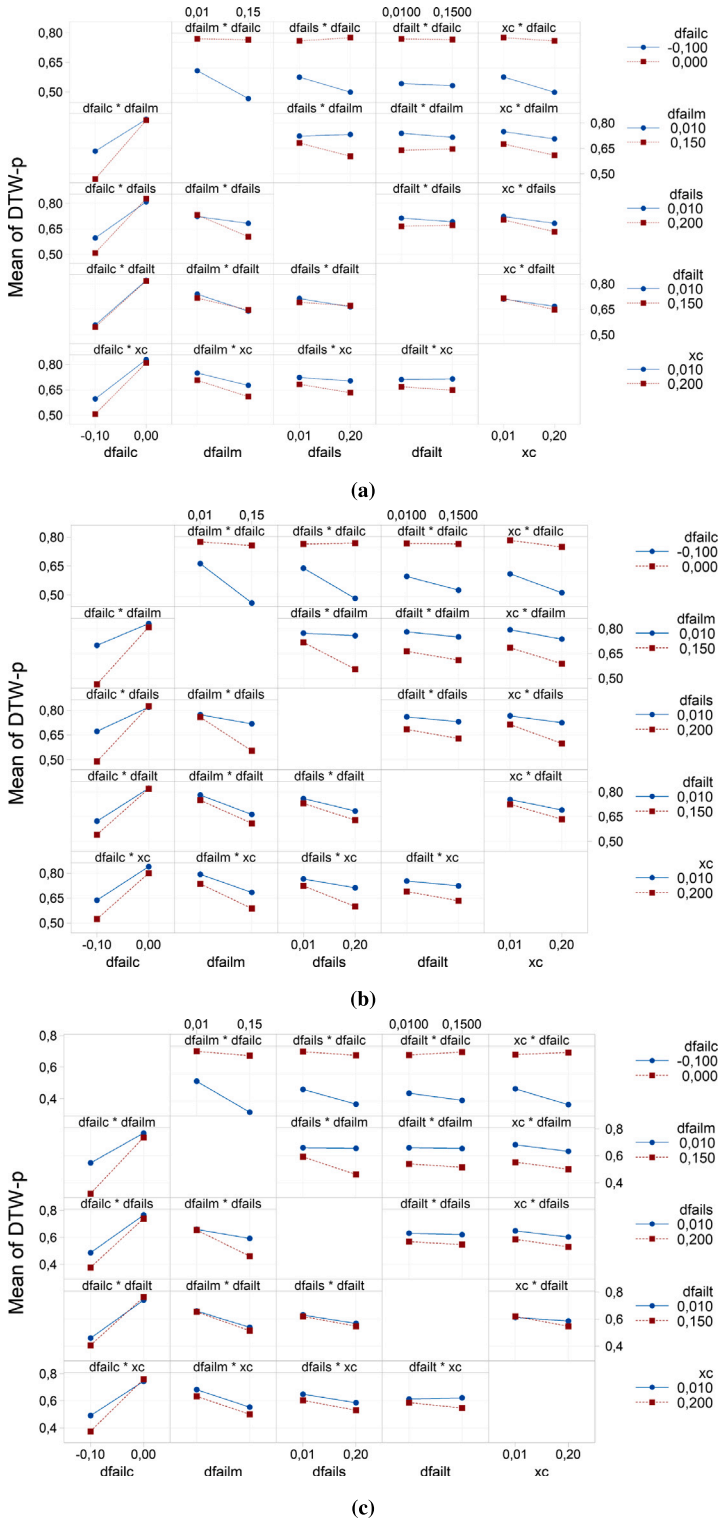

Fig. 11. Interaction plots for DTW-p response for Flax cases at (a) 5 J, (b) 10 J, and (c) 15 J.

Thus, the optimization results are highly dependent on the boundary conditions.

7.2.2. *Multi-target optimization*

To obtain results that generalize well, we consider here an LS-OPT setup that considers all three loading scenarios simultaneously. In addition to the previous parameters, the variable XC is also included in the optimization procedure, since it is the third relevant term in the sensitivity analysis of the 5 J case. Starting from the trial-and-error configuration, we apply EGO on a four-dimensional domain, considering 20 DoE samples and 100 evaluations for the iterative phase. The objective function now corresponds to the sum of the curvematching functions defined for each energy level. We performed three repetitions of the optimization run with different random seeds to statistically validate the procedure. From now on, our discussion will refer to the one that yielded the minimum value of the objective function.

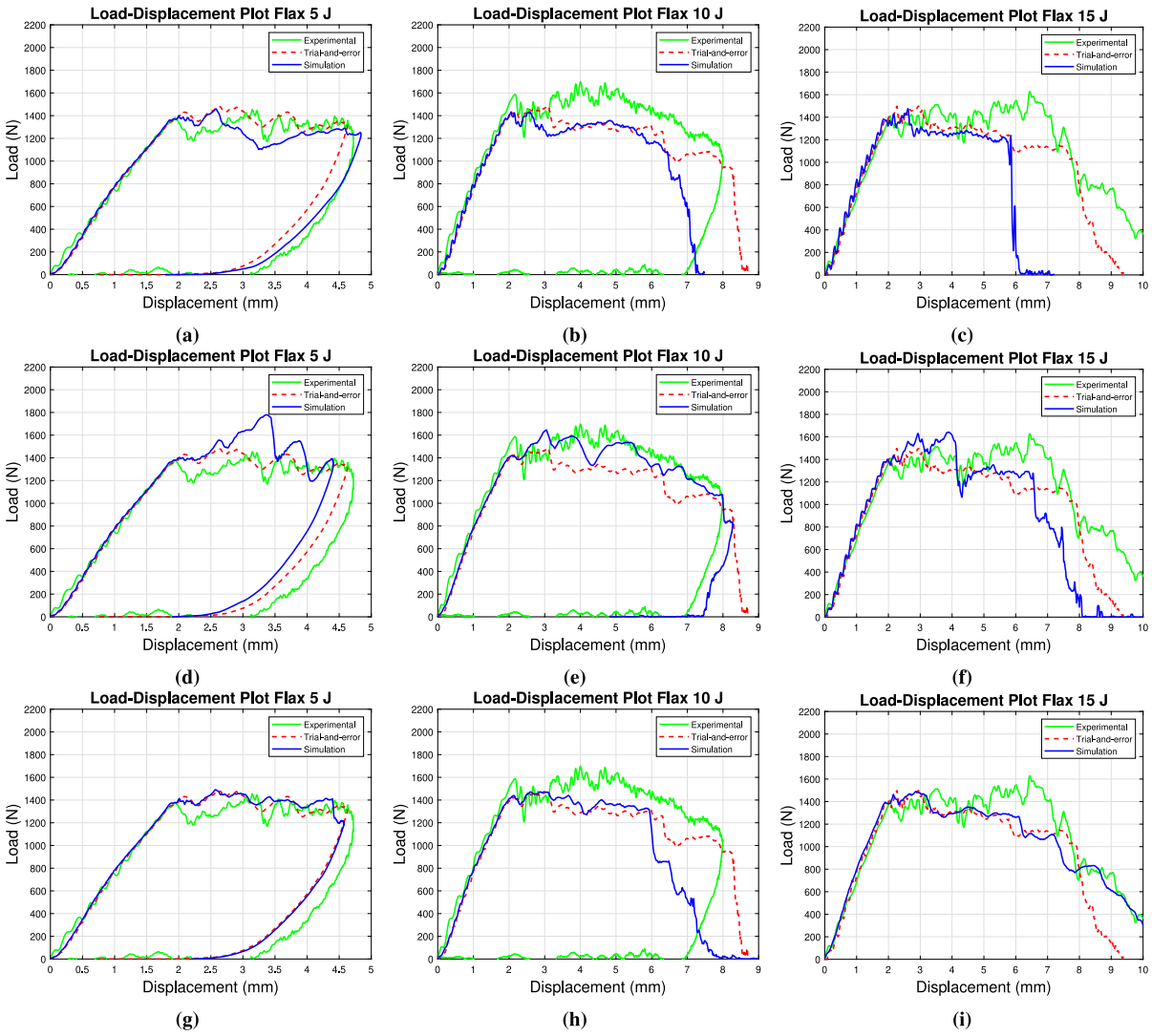

Fig. 12. Comparison between the experimental, the trial-and-error and the numerical load–displacement curves obtained with the optimal set of parameters for the cases (a-c) 5 J, (d-f) 10 J, and (g-i) 15 J.

Fig. 13(a) shows the optimization history of both the infill point and the best point computed at each iteration. The series of the best-computed points decreases monotonically since the orange marker is updated only when the new infill point has a better objective function value than the previous best point [34].

In this case, EGO converges to an optimum at iteration 89, with optimal solution (DFAILC, DFAILM, DFAILS, XC) = $(-0.0599016, 0.101414, 0.170736, 0.150792)$. To validate the result for each test case, a FEM simulation is performed in LS-DYNA to verify that the optimal values are able to reproduce the experimental load–displacement trend for all tested energy levels.

The obtained curves are shown in Fig. 14, where we observe a good agreement between the numerical and experimental curves, regardless of the level of impact energy. Moreover, a clear improvement in the trend over the curves obtained by trial and error is evident. Hence, the multi-target approach provides an optimal parameter configuration that is less sensitive to the specific energy level, thus proving to be a very powerful tool for material characterization. Note that the global optimum found using the EGO strategy for the multi-target approach does not match the optimum for the 5 J single scenario. This is evident from the plots in Figs. 13(b), 13(c), and 13(d), which show the evolution of the curvematching values for each energy level. In fact, the orange markers do not decrease monotonically with iterations, showing that the optimal solution found considering the multi-target is not necessarily optimal for a given impact energy level. However, in terms of material characterization, it is better to consider a robust optimum that does not depend on the boundary conditions, rather than the optimum for a particular energy level.

We also validate the optimized model, checking its ability to reproduce the evolution of the absorbed energy as a function of displacement during the impact test, which is shown in Fig. 15. For completeness, the parameters of the numerical model derived from the EGO run with the best target value, and therefore used to characterize the flax/epoxy laminates subjected to the LVI tests, are shown in Table 4.

To evaluate the accuracy of the numerical curve compared to the experimental curve, three different statistical error measurements are evaluated: the Root Mean Squared Error (RMSE), the coefficient of determination (R^2), and the maximal residual error (ϵ_{max}). These values must be small enough, except for R^2 where a value close to the unit is required to accept the accuracy of the predicted values. The numerical curve for the model tuned by trial and error is always less accurate than the optimized curve with respect to any error measure, which proves the improvement led by the optimization process. The only exception is the case at 5 J, where there is no improvement because the trial-and-error configuration already showed good agreement between the experimental and numerical load–displacement curves. Fig. 16 provides

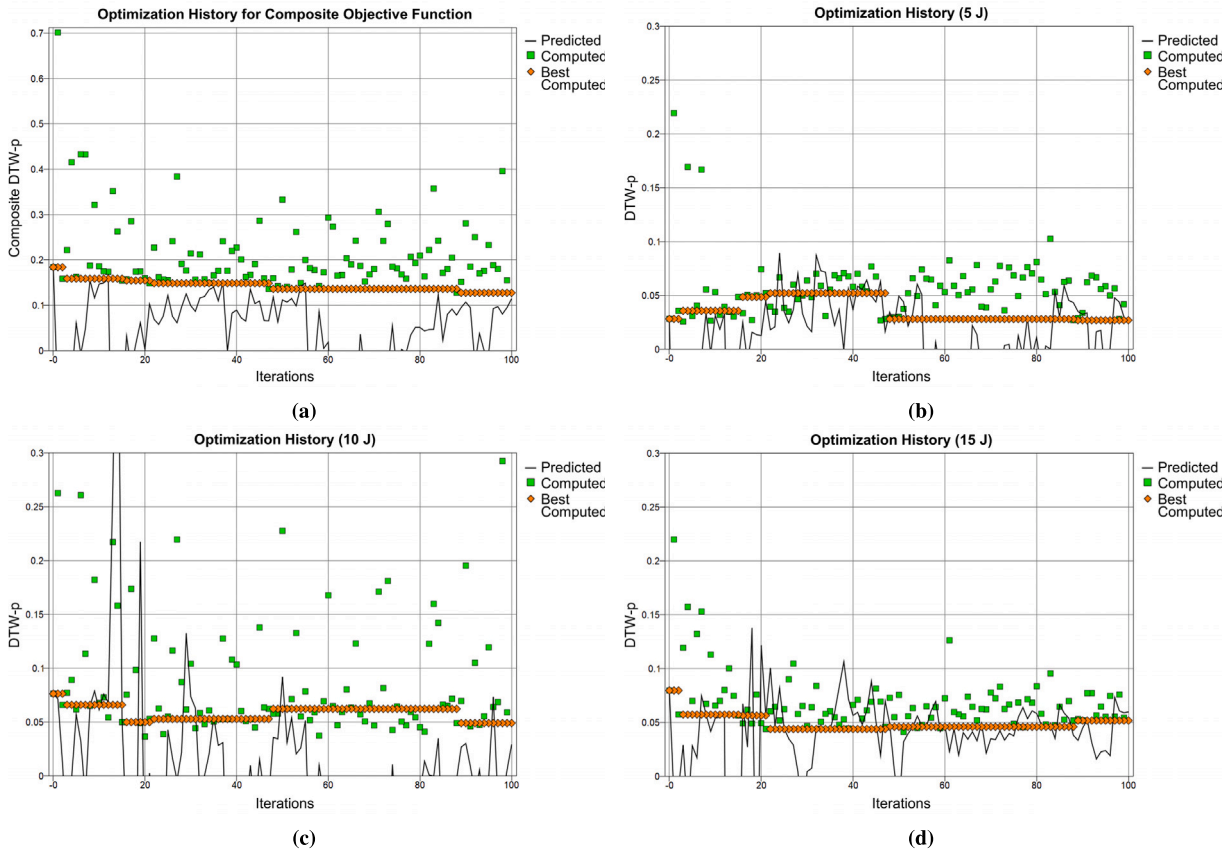

Fig. 13. Optimization histories of the multi-target EGO algorithm showing the convergence of (a) the composite target, and the curvematching target for the single energy level: (b) 5 J, (c) 10 J, and (d) 15 J. Both the histories of the infill point and the best computed are shown, together with value evaluated on the predicted model for each infill point.

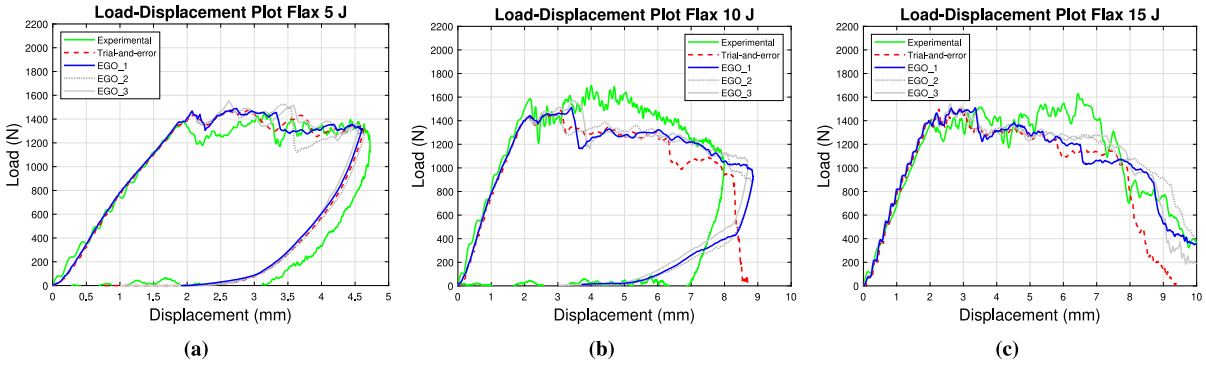

Fig. 14. Comparison between the experimental curve, the trial-and-error curve, and the optimized load–displacement curves for flax samples impacted at (a) 5 J, (b) 10 J and (c) 15 J. In blue, is the curve resulting from simulating the model with the parameter configuration that yields the best target (DTW) optimization. In gray are the curves from the other repetitions.

Table 4
MAT54/55 Material properties for flax laminates. See [27] for parameters description.

MAT_ENHANCED_COMPOSITE_DAMAGE (MAT54/55)						
RO (Kg/mm^3)	**EA (GPa)**	**EB (GPa)**	**PRBA**	**GAB (GPa)**	**GBC (GPa)**	**GCA (GPa)**
1.29E−6	10.3	10.3	0.17	1.8	0.3	0.3
DFAILM	**DFAILS**	**DFAILT**	**DFAILC**			
0.101414	0.170736	0.0885269	−0.0599016			
XC (GPa)	**XT (GPa)**	**YC (GPa)**	**YT (GPa)**	**SC (GPa)**		
0.150792	0.12	0.150792	0.12	0.0304		

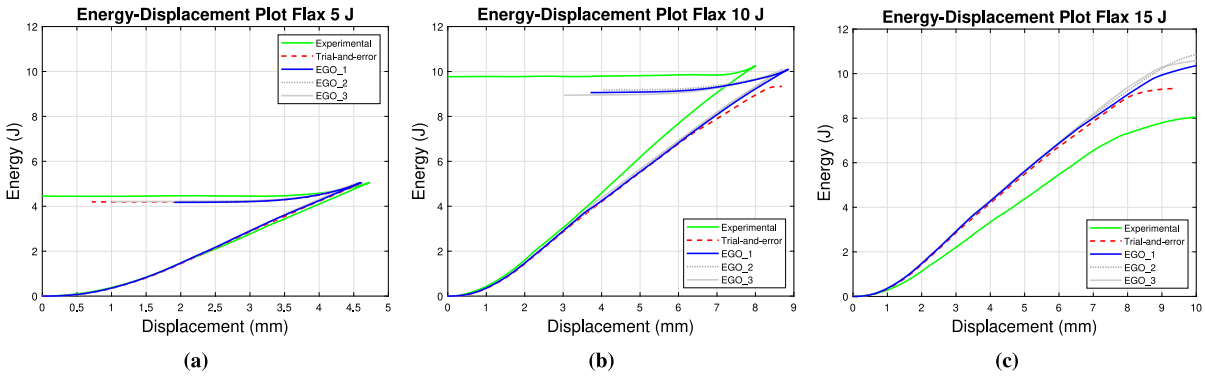

Fig. 15. Comparison between the experimental curve, the trial and error curve, and the optimized energy–displacement curves for flax samples impacted at (a) 5 J, (b) 10 J, and (c) 15 J. In blue, the curve resulting from simulating the model with the parameter configuration that yields the best target (DTW) optimization. In gray the curves from the other repetitions.

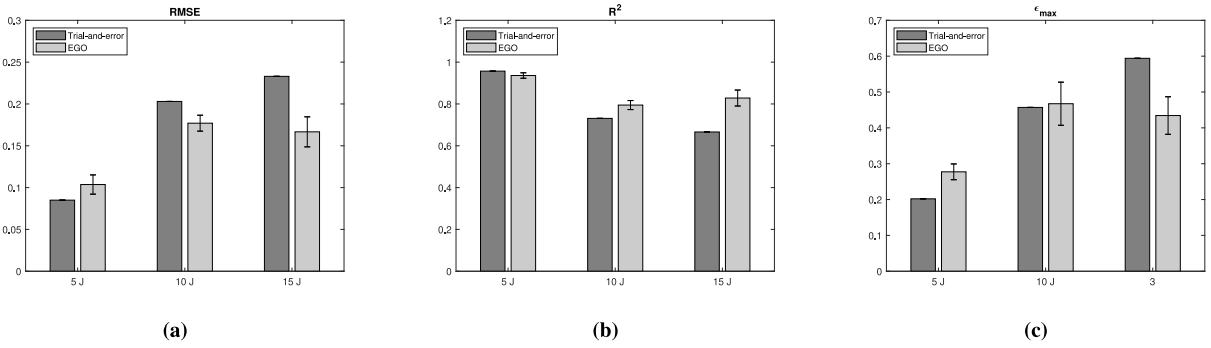

Fig. 16. Evaluation of the accuracy measures: (a) RMSE, (b) R^2, (c) ϵ_{max}. For the EGO bars, mean and standard deviation computed over the three repetitions of the optimization procedure are shown.

visual evidence. Accuracy metrics are evaluated for each energy level and their mean and standard deviation are given in the figure.

Agreement in terms of force–displacement curves does not guarantee agreement in terms of failure modes [35]. Therefore, we also provide evidence for agreement between numerical and experimental results with respect to damage. Fig. 17 illustrates the numerical damage evolution on the back surfaces (Fig. 17(a)) and on the front surfaces (Fig. 17(b)) of the laminates, with stress distribution, obtained from the optimized models for each impact energy level.

The finite element models are able to capture the experimental cross-shaped crack propagation, although the numerical openings are more pronounced compared to the experimental results. This is due to the fact that the model consists of 4 layers instead of 8, and thus the damage leads to an easier deletion of the elements. This suggests that a more complex numerical model with the same number of layers as the experimental samples might be able to better reproduce the damage phenomenon and therefore deserves further investigation. We note that despite the differences in damage propagation, the simplified model does not involve any perturbation of the optimal values for the material parameters studied. In fact, each layer of the numerical model has two integration points and twice the thickness of the average layer in the experimental specimens, which enables it to reproduce the experimental setup accurately while saving computational time.

8. Conclusions

This paper presents experimental results and a numerical optimization study to identify the material parameters of a flax/epoxy resin composite laminate under different low-velocity impact conditions. Although many parameters of a composite material card can be determined by experimental testing, others must be tuned by hand because they are non-physical or simply unavailable from experimental testing. However, the trial-and-error technique is often very time-consuming and relies excessively on the experience of the designer. Our goal was to find an optimal parameter configuration that could accurately predict the experimental force–displacement and energy–displacement curves and numerically reproduce the observed damage mechanisms. Our investigation mainly focused on five material card parameters – DFAILM, DFAILT, DFAILC, DFAILS, and XC – which were reduced to four after sensitivity analysis. Hence, we performed an optimization study using the external optimization tool LS-OPT, where dynamic time warping was chosen as a similarity measure for three different levels of impact energy: 5, 10, and 15 J. An iterative optimization strategy using the Efficient Global Optimization (EGO) algorithm was used to obtain optimal parameter values by keeping the number of function evaluations, i.e., numerical simulations, as low as possible. A limitation of the EGO algorithm is that it suffers from significant computational complexity and a lower convergence rate as the dimension of the problem increases. However, in this study, we were able to reduce the dimension of the parameter space to four variables through an initial screening of the influential parameters and the sensitivity analysis phase.

After performing three different optimizations for the three energy levels, we found that this strategy provides a good prediction of the experimental LVI behavior of flax/epoxy composites only for the energy level for which the optimization is performed. Hence, we considered the multi-target approach, which provides a final robust optimum across different energy levels, showing the potential of EGO for material characterization. Our results show that the simulations performed with the optimized models provide load–displacement and energy–displacement curves that reproduce the experimental behavior for each energy level with higher accuracy than the simulations performed with the hand-tuned numerical models, and in much less time. This was evident from both visual inspection of the resulting curves

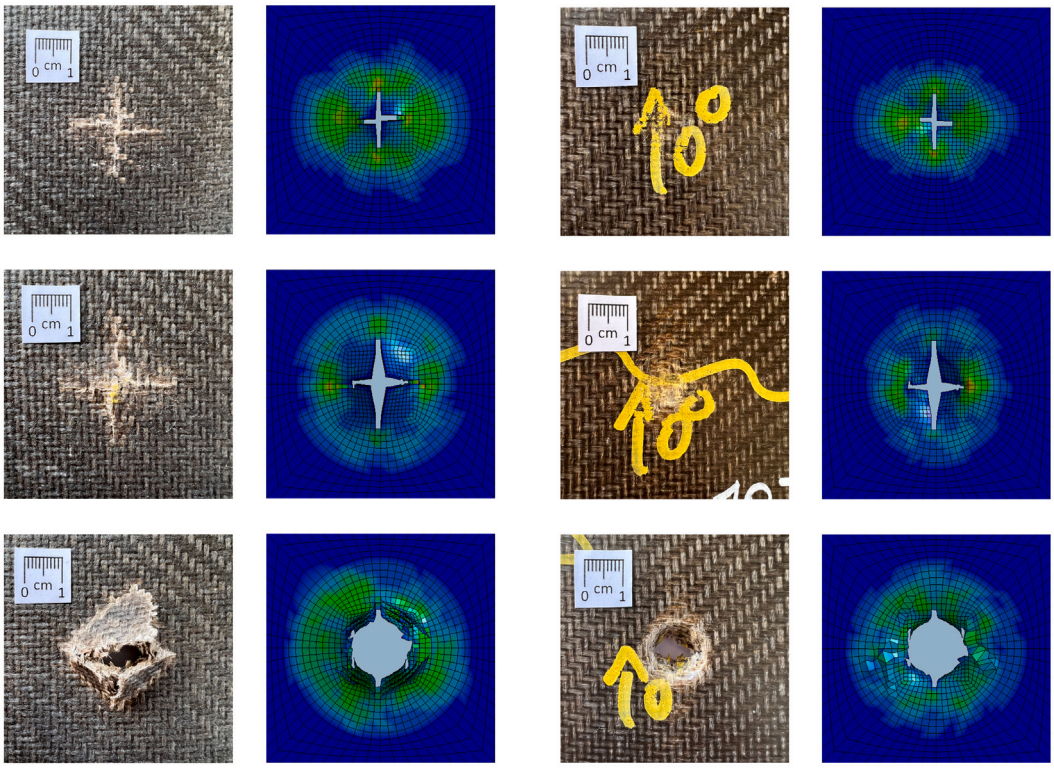

Fig. 17. Comparison of crack propagation on the back (a) and front (b) surfaces between experimental test and numerical simulation for samples impacted at 5 J, 10 J, and 15 J.

and measurement of accuracy. Moreover, the optimized models are able to reproduce the experimentally observed damage mechanisms for all impact energies. More generally, this study allowed the material characterization of flax-fiber/epoxy-resin composite laminates using a MAT54/55 card, specifically designed for unidirectional laminates, but representing a good compromise between accuracy and optimization efficiency compared to material cards for woven composites, which are characterized by many more parameters to be adjusted.

CRediT authorship contribution statement

Valentina Giammaria: Conceptualization, Methodology, Software, Investigation, Data curation, Writing – original draft, Writing – review & editing, Visualization. **Giulia Del Bianco:** Conceptualization, Methodology, Software, Investigation, Writing – original draft, Writing – review & editing, Visualization. **Elena Raponi:** Conceptualization, Methodology, Software, Investigation, Writing – original draft, Writing – review & editing, Visualization. **Dario Fiumarella:** Investigation, Writing – review & editing. **Raffaele Ciardiello:** Investigation, Writing – review & editing. **Simonetta Boria:** Conceptualization, Investigation, Writing – review & editing, Supervision. **Fabian Duddeck:** Conceptualization, Investigation, Writing – review & editing, Supervision. **Giovanni Belingardi:** Conceptualization, Resources, Writing – review & editing, Supervision.

Declaration of competing interest

The authors declare that they have no known competing financial interests or personal relationships that could have appeared to influence the work reported in this paper.

Data availability

Data will be made available on request

Acknowledgments

The authors would like to thank HP Composites SpA for the realization and provision of the laminate materials. The authors also thank Prof. Alessandro Scattina for the assistance in the experimental tests carried out with professional equipment in the laboratories of Politecnico di Torino. Elena Raponi acknowledges funding by the PRIME programme of the German Academic Exchange Service (DAAD) with funds from the German Federal Ministry of Education and Research (BMBF).

References

[1] Naqvi SR, Prabhakara HM, Bramer EA, Dierkes W, Akkerman R, Brem G. A critical review on recycling of end-of-life carbon fibre/glass fibre reinforced composites waste using pyrolysis towards a circular economy. Resour Conserv Recy 2018;136:118–29. http://dx.doi.org/10.1016/j.resconrec.2018.04.013.

[2] Joshi SV, Drzal LT, Mohanty AK, Arora S. Are natural fiber composites environmentally superior to glass fiber reinforced composites? In: AIChE 2002, Composites A In: AIChE 2002, 2004;35(3):371–6.http://dx.doi.org/10.1016/j.compositesa.2003.09.016,

[3] Ku H, Wang H, Pattarachaiyakoop N, Trada M. A review on the tensile properties of natural fiber reinforced polymer composites. Composites B 2011;42(4):856–73. http://dx.doi.org/10.1016/j.compositesb.2011.01.010.

[4] Bensadoun F, Vanderfeesten B, Verpoest I, Van Vuure AW, Van Acker K. Environmental impact assessment of end of life options for flax-MAPP composites. Ind Crops Prod 2016;94:327–41. http://dx.doi.org/10.1016/j.indcrop.2016.09.006.

[5] Shahzad A. Hemp fiber and its composites – a review. J Compos Mater 2012;46(8):973–86. http://dx.doi.org/10.1177/0021998311413623.

[6] Yan L, Chouw N, Jayaraman K. Flax fibre and its composites – A review. Composites B 2014;56:296–317. http://dx.doi.org/10.1016/j.compositesb.2013.08.014.

[7] Sliseris J, Yan L, Kasal B. Numerical modelling of flax short fibre reinforced and flax fibre fabric reinforced polymer composites. Composites B 2016;89:143–54. http://dx.doi.org/10.1016/j.compositesb.2015.11.038.

[8] Pickering KL, Efendy MGA, Le TM. A review of recent developments in natural fibre composites and their mechanical performance. In: Special issue on biocomposites, Composites A In: Special issue on biocomposites, 2016;83:98–112.http://dx.doi.org/10.1016/j.compositesa.2015.08.038,

[9] Fiore V, Scalici T, Calabrese L, Valenza A, Proverbio E. Effect of external basalt layers on durability behaviour of flax reinforced composites. Composites B 2016;84:258–65. http://dx.doi.org/10.1016/j.compositesb.2015.08.087.
[10] Raponi E, Boria S, Giammaria V, Fischer B, Pörnbacher J, Sarasini F, et al. Effect of basalt intraply hybridization on the damage tolerance of flax laminates: Experimental analysis and analytical modeling under low-velocity impact. Compos Struct 2022;287:115270. http://dx.doi.org/10.1016/j.compstruct.2022.115270.
[11] Fiore V, Valenza A, Di Bella G. Mechanical behavior of carbon/flax hybrid composites for structural applications. J Compos Mater 2012;46(17):2089–96. http://dx.doi.org/10.1177/0021998311429884.
[12] Arbelaiz A, Fernández B, Cantero G, Llano-Ponte R, Valea A, Mondragon I. Mechanical properties of flax fibre/polypropylene composites. Influence of fibre/matrix modification and glass fibre hybridization. Composites A 2005;36(12):1637–44. http://dx.doi.org/10.1016/j.compositesa.2005.03.021.
[13] Morye S, Wool R. Mechanical properties of glass/flax hybrid composites based on a novel modified soybean oil matrix material. Polym Compos 2005;26(4):407–16. http://dx.doi.org/10.1002/pc.20099.
[14] Zhang Y, Li Y, Ma H, Yu T. Tensile and interfacial properties of unidirectional flax/glass fiber reinforced hybrid composites. Compos Sci Technol 2013;88:172–7. http://dx.doi.org/10.1016/j.compscitech.2013.08.037.
[15] Kumar S, Venkatesh D, Subbaratnam B, Shekar M. Mechanical testing and numerical analysis of flax/glass epoxy hybrid composite material. IOP Conf Ser Mater Sci Eng 2020;998:012032. http://dx.doi.org/10.1088/1757-899X/998/1/012032.
[16] Shen Y, Zhong J, Cai S, Ma H, Qu Z, Guo Y, et al. Effect of temperature and water absorption on low-velocity impact damage of composites with multilayer structured flax fiber. Materials 2019;12(3):453. http://dx.doi.org/10.3390/ma12030453.
[17] Raponi E, Sergi C, Boria S, Tirillò J, Sarasini F, Calzolari A. Temperature effect on impact response of flax/epoxy laminates: Analytical, numerical and experimental results. Compos Struct 2021;274:114316. http://dx.doi.org/10.1016/j.compstruct.2021.114316.
[18] Liang S, Gning P-B, Guillaumat L. Quasi-static behaviour and damage assessment of flax/epoxy composites. Mater Des 2015;67:344–53. http://dx.doi.org/10.1016/j.matdes.2014.11.048.
[19] Poilâne C, Cherif ZE, Richard F, Vivet A, Ben Doudou B, Chen J. Polymer reinforced by flax fibres as a viscoelastoplastic material. Compos Struct 2014;112:100–12. http://dx.doi.org/10.1016/j.compstruct.2014.01.043.
[20] Assarar M, Zouari W, Sabhi H, Ayad R, Berthelot J-M. Evaluation of the damping of hybrid carbon–flax reinforced composites. Compos Struct 2015;132:148–54. http://dx.doi.org/10.1016/j.compstruct.2015.05.016.
[21] Sy BL, Fawaz Z, Bougherara H. Numerical simulation correlating the low velocity impact behaviour of flax/epoxy laminates. Composites A 2019;126:105582. http://dx.doi.org/10.1016/j.compositesa.2019.105582.
[22] Mocerino D, Boccarusso L, Fazio D, Durante M, Langella A, Meo M, et al. Prediction of the impact behavior of bio-hybrid composites using finite element method. In: ESAFORM 2021. 2021, http://dx.doi.org/10.25518/esaform21.2651.
[23] Abrate S. Impact on composite structures. Cambridge: Cambridge University Press; 1998, http://dx.doi.org/10.1017/CBO9780511574504.
[24] Mulenga T, Ude A, Chinnasamy V. Fibers techniques for modelling and optimizing the mechanical properties of natural fiber composites: A review. Fibers 2021;9:6. http://dx.doi.org/10.3390/fib9010006.
[25] Jones DR, Schonlau M, Welch WJ. Efficient global optimization of expensive black-box functions. J Global Optim 1998;13(4):455–92. http://dx.doi.org/10.1023/A:1008306431147.
[26] LS-Opt user manual. A design optimization and probabilistic analysis tool for the engineering analyst, Version 6.0, Livermore Software Technology Corporation. 2019.
[27] LS-DYNA keyword user's manual. Vol. II. Material models, r12 ed.. Livermore Software Technology; 2020.
[28] Feraboli P, Wade B, Deleo F, Rassaian M, Higgins M, Byar A. LS-DYNA MAT54 modeling of the axial crushing of a composite tape sinusoidal specimen. Composites A 2011;42(11):1809–25. http://dx.doi.org/10.1016/j.compositesa.2011.08.004.
[29] Ahmed S, Ulven CA. Dynamic in-situ observation on the failure mechanism of flax fiber through scanning electron microscopy. Fibers 2018;6(1):17. http://dx.doi.org/10.3390/fib6010017.
[30] Cherniaev A, Butcher C, Montesano J. Predicting the axial crush response of CFRP tubes using three damage-based constitutive models. Thin-Walled Struct 2018;129:349–64. http://dx.doi.org/10.1016/j.tws.2018.05.003.
[31] Forrester AIJ, Sóbester A, Keane AJ. Engineering design via surrogate modelling - A practical guide. John Wiley & Sons Ltd; 2008, http://dx.doi.org/10.1002/9780470770801.
[32] Witowski K, Stander N. Modified dynamic time warping for utilizing partial curve data to calibrate material models. 2020, p. 9.
[33] Raponi E, Bujny M, Olhofer M, Aulig N, Boria S, Duddeck F. Kriging-assisted topology optimization of crash structures. Comput Methods Appl Mech Engrg 2019;348:730–52. http://dx.doi.org/10.1016/j.cma.2019.02.002, URL: https://www.sciencedirect.com/science/article/pii/S0045782519300726.
[34] Raponi E, Fiumarella D, Boria S, Scattina A, Belingardi G. Methodology for parameter identification on a thermoplastic composite crash absorber by the sequential response surface method and efficient global optimization. Compos Struct 2021;278:114646. http://dx.doi.org/10.1016/j.compstruct.2021.114646, URL: https://linkinghub.elsevier.com/retrieve/pii/S0263822321011053.
[35] Dong S, Sheldon A, Carney K. Modeling of carbon-fiber-reinforced polymer (CFRP) composites in LS-DYNA® with optimization of material and failure parameters in LS-OPT®. 2018.